11th World Congress on Computational Mechanics (WCCM XI)
5th European Conference on Computational Mechanics (ECCM V)
6th European Conference on Computational Fluid Dynamics (ECFD VI)
E. Oñate, J. Oliver and A. Huerta (Eds)

DEVELOPMENT OF A COHESIVE MODEL FOR DAMAGE SIMULATION IN FERROELECTRIC MATERIALS SUBJECTED TO ELECTROMECHANICAL LOADING

S. KOZINOV[†*], S. ROTH[†], M. KUNA[†]

[†] Institute for Mechanics and Fluid Dynamics, TU Bergakademie Freiberg
Lampadiusstraße 4, 09596, Germany
Sergii.Kozinov@imfd.tu-freiberg.de, Stephan.Roth@imfd.tu-freiberg.de,
Meinhard.Kuna@imfd.tu-freiberg.de URL: http://tu-freiberg.de/fakult4/imfd/fkm/

[*] Department of Theoretical and Applied Mechanics, Dnipropetrovsk National University
Gagarina 72, 49010, Ukraine, URL: http://www.dnu.dp.ua/en

Key Words: Cohesive Zone Model, Ferroelectric Domain Switching, Fracture, Finite Element Method.

Abstract. Fracture of ferroelectric materials is studied numerically using an advanced exponential cyclic cohesive zone model. The implemented irreversible cohesive law allows damage accumulation during (re)loading. Change in polarization direction (as a result of possible switching of ferroelectric domains) around cracks due to applied electromechanical loading is considered. In order to represent the permittivity of the grain boundaries or the crack faces a parallel plate capacitor model is implemented into the cohesive law. Numerical simulations are performed for the basic test model as well as for a crack in ferroelectric bulk material. The results show realistic electric field influence on the fracture toughness of the specimen as well as crack initiation and growth pattern. Mechanisms of the crack initiation and propagation in the ferroelectric medium under cyclic electric loading of constant amplitude are illustrated.

1. INTRODUCTION

Brittleness and sensitivity to fracture of piezoelectric ceramics has an impact on reliability of sensors, transducers and actuators. Their unexpected failure can be caused by high mechanical stresses or electrical fields. The problem of fracture in piezoelectric ceramics during manufacturing or under cyclic electric loading is quite complex and far from being exhaustively understood. Therefore, to increase reliability of smart materials and structures it is very important to create a sound model to asses fracture behavior of ferroelectric ceramics.

Progress in simulation of ferroelectric ceramics cracking is summarized in reviews [1, 2]. Many currently presented models are quite complex but still not exhaustive since the microstructural behavior is not realistically formulated. Even nowadays the failure phenomena occurring at the grain level during subcritical electrical or mechanical loading are not well understood. Therefore, more realistic local failure concepts and simulation tools are

required to evaluate crack initiation and growth at field concentrations like crack tips. Models of this kind are highly demanded for reliable and safe operation of piezoelectric devices.

According to [3] amorphous structures with reduced coupled electromechanical effects emanate as a result of damage of the macroscopic ferroelectric polycrystals. It is considered [4], that ferroelectric fatigue is driven by electrical, mechanical, electro-chemical mechanisms and the influence of each of them is difficult to separate. According to the experiments [5], a nominal threshold value of ΔE exists to activate fatigue crack initiation.

One of the very promising approaches to simulate damage initiation and evolution is the cohesive zone model. In addition to the pure mechanical behavior of the cohesive zone material, for piezoelectric ceramics the dielectric material properties have to be taken into account. It is well known that the electric properties of the crack filler (air, water, silicon oil, etc.) can be taken into consideration by appropriate crack face boundary conditions. Synthesizing two limiting cases of electrically permeable or impermeable crack faces, realistic limited permeable crack media boundary conditions were proposed [6, 7].

A first extension of cohesive zone models to piezoelectric/ferroelectric materials was made in [8]. A basic exponential cohesive law was combined with a ferroelectric material behavior in a one-dimensional setting to simulate electric fatigue of bulk samples. However, physically questionable is an explicit inclusion of the electric potential jump into the cohesive effective separation. In [9] simulations of cohesive fatigue effects in a linear piezoelectric mesostructure were performed. A constitutive cohesive zone model for piezoelectric bulk behavior under mechanical loading allowing for discontinuities both in the elastic displacements and the electric potential along the element boundaries was developed in [10].

In the above mentioned papers [8-10] only two-dimensional cracked bodies and cohesive elements are considered besides that most of the cohesive zone models do not take into account a progressive damage during subcritical electromechanical loading.

The present paper attempts to overcome the aforementioned limitations, combining all the required demands in a single approach by using a non-linear ferroelectric bulk behavior (domain switching) and an enhanced electromechanical cyclic cohesive law for three-dimensional analyses of the electromechanical fracture.

2. CONSTITUTIVE BEHAVIOR OF FERROELECTRIC MATERIALS

In the absence of body forces and free electrical charges the equilibrium equations for a ferroelectric material in a fixed rectangular coordinate system x_k (k = 1-3) have the form:

$$\sigma_{ij,j} = 0, \;\; D_{j,j} = 0. \tag{1}$$

Constitutive equations are

$$\sigma_{ij} = C_{ijkl}(\varepsilon_{kl} - \varepsilon_{kl}^r) - e_{lij}E_l, \tag{2}$$

$$D_i = e_{ikl}(\varepsilon_{kl} - \varepsilon_{kl}^r) + \kappa_{il}E_l + P_i^r. \tag{3}$$

Kinematic equations are

$$\varepsilon_{ij} = \left(u_{i,j} + u_{j,i}\right)/2, \;\; E_i = -\varphi_{,i}, \tag{4}$$

where $u_k, \varepsilon_{ij}, \varphi, \sigma_{ij}, D_i, E_i$ are elastic displacements, elastic strains, electric potential, stresses, electric displacements and electric field components, respectively. ε_{kl}^r and P_i^r are the remanent strain and polarization. The coefficients C_{ijkl} are the elastic constants, e_{ikl} are the

piezoelectric constants and κ_{il} are the dielectric permittivities. In equations (1)-(4) the indices are ranging from 1 to 3 and a comma denotes partial differentiation.

Domains are subregions of a crystalline grain where all dipole moments of neighboring unit cells are oriented in the same direction. The unit cell for a single tetragonal ferroelectric crystal is depicted in Fig. 1. There are possibilities for 180° domain switching leading to the remanent polarization change with no influence on the remanent strain value, and 90° switching affecting both remanent strain and polarization. By means of nonlinear evolution laws the polarization and strain hysteresis in ferroelectric materials can be described as a result of switching (Fig. 2).

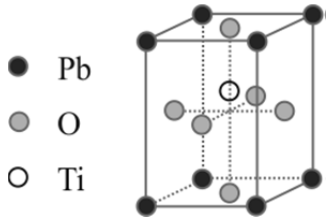

Figure 1. Tetragonal unit cell.

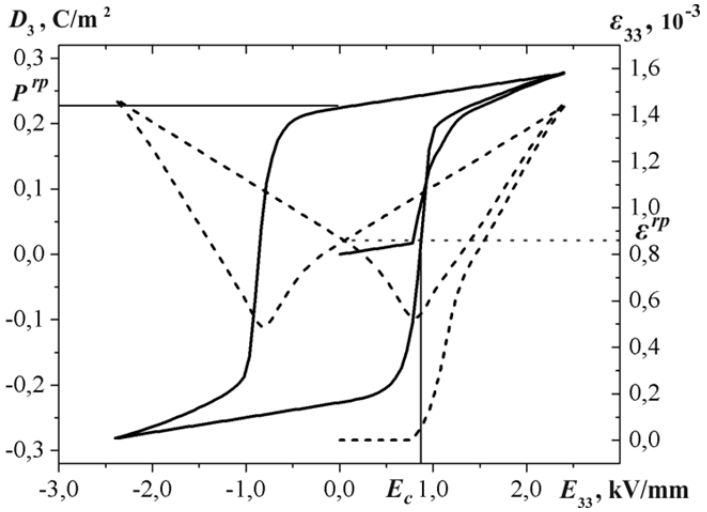

Figure 2. Strain (dashed) and polarization (solid) hysteresis loops.

The alignment of domains in the grains during polarization is illustrated in Fig. 3a. Due to the applied external electric field, domains orient along the direction of the electric field (Fig. 3b) and after the removal of the field a macroscopic polarization remains (Fig. 3c).

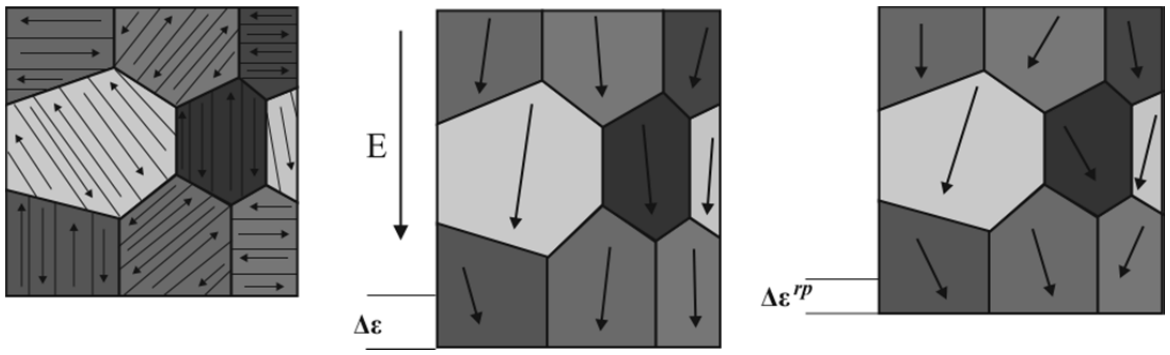

a) b) c)

Figure 3. Domains reorientation during polarization
(Δε – strain in a representative polycrystalline volume element, $\Delta\varepsilon^{rp}$ - remanent macro strain).

In the present paper, a user-defined material routine [11] is used for the modeling of micromechanical tetragonal domain switching.

Every domain type is represented by a volume fraction $v^{(N)}$ $(N = 1, 2, 3, 4, 5, 6)$. Strain and

electric displacement along with their remanent values are calculated by volume averaging over the six tetragonal domain variants:

$$\varepsilon_{kl} = \sum_{N=1}^{6} \varepsilon_{kl}^{(N)} \nu^{(N)}, \quad \varepsilon_{kl}^{r} = \sum_{N=1}^{6} \varepsilon_{kl}^{r(N)} \nu^{(N)}, \quad D_i = \sum_{N=1}^{6} D_i^{(N)} \nu^{(N)}, \quad D_i^{r} = \sum_{N=1}^{6} D_i^{r(N)} \nu^{(N)} \tag{5}$$

and effective material properties are found as following:

$$S_{ijkl} = \sum_{N=1}^{6} S_{ijkl}^{(N)} \nu^{(N)}, \quad e_{ikl} = \sum_{N=1}^{6} e_{ikl}^{(N)} \nu^{(N)}, \quad \kappa_{il} = \sum_{N=1}^{6} \kappa_{il}^{(N)} \nu^{(N)}, \tag{6}$$

where S_{ijkl} are the elastic compliances.

The switching criterion used for each of the six domains is based on requirement of energy supply to overcome energy barrier [12]:

$$\sigma_{ij}\varepsilon_{ij} + \sigma_{ij}\Delta\varepsilon_{ij}^{sp} + E_i D_i + E_i \Delta P_i^{sp} \geq \omega_c, \tag{7}$$

where $\Delta\varepsilon_{ij}^{sp}$ – change of the spontaneous strain, ΔP_i^{sp} – change of the spontaneous polarization. According to [2] the critical work for $\pm 90°$ and for $180°$ domain switching is

$$\omega_c^{\pm 90°} = \sqrt{2} P^{sp} E_c, \quad \omega_c^{180°} = 2 P^{sp} E_c, \tag{8}$$

where E_c – coercive electric field strength of ferroelectric material.

Polarization and strain hysteresis loops are calculated for lead zirconate titanate PZT-5H polycrystal subjected to cyclic electric field alternating from 0 to $3E_c$. Results of the simulation are shown in Fig. 2. The coercive field $3E_c$ = 0.8 kV/mm, the remanent strain ε^{rp} = $0.85 \cdot 10^{-3}$ and the remanent polarization in the polycrystal P^{rp} = 0.23 C/m^2 can be found in the presented diagram.

3. ELECTROMECHANICAL CYCLIC COHESIVE ZONE MODEL

3.1. Basic ideas

One of the most efficient methods for numerical simulation of fracture processes is the cohesive zone approach. Using this approach, the whole damage process, starting with the crack initiation until overall failure, can be modelled. As an extension of previously developed mechanical cyclic cohesive zone model [13, 14] in the current paper an electromechanical cyclic cohesive zone model (EMCCZM) is presented. Exhaustive explanation about the developed ECCCZM can be found in [15].

Fig. 4 explains cohesive zone approach and parallel plate capacitor model. Point A corresponds to the maximum cohesive traction at which critical separation δ_0 occurs. Point B describes completely damaged material. In Fig. 4 (right), t^* and ω^* represent mechanical and electrical loading at the cohesive element faces associated with the dielectric properties of the cohesive zone.

The cohesive element behavior consists of a monotonic and cyclic traction-separation law (TSL) as well as an electromechanical coupling described in subsections 3.2 – 3.4.

3.2. Monotonic traction-separation law

Normalized effective traction t and separation δ are defined by the formula:

$$t = \sqrt{t_n^2 + t_r^2 + t_s^2}/t_0, \quad \delta = \sqrt{\langle\delta_n\rangle^2 + \delta_r^2 + \delta_s^2}/\delta_0, \tag{9}$$

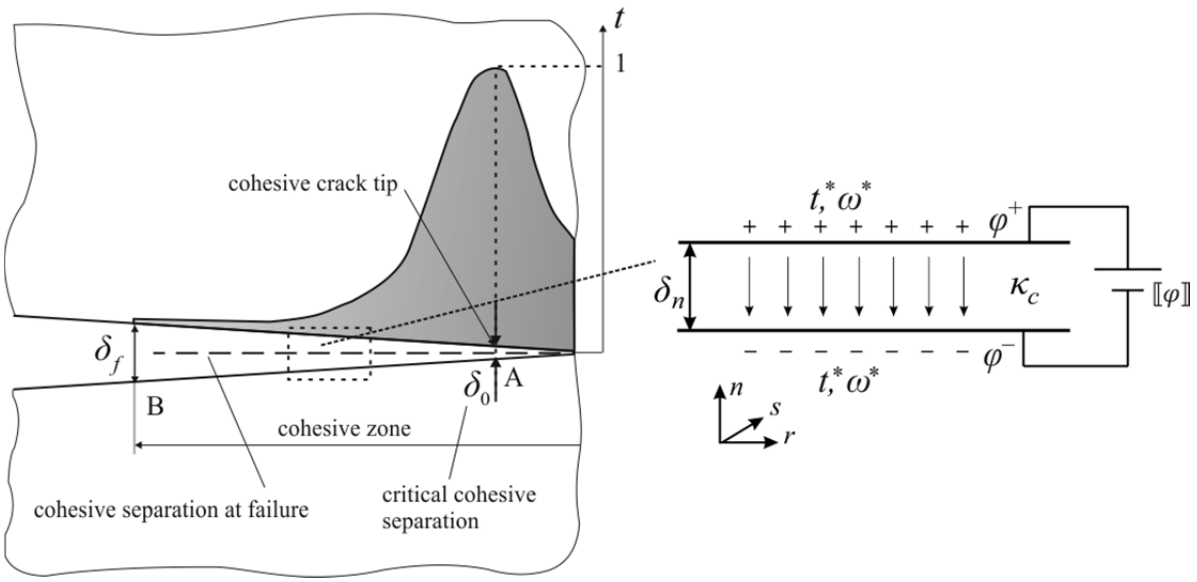

Figure 4. Cohesive zone modeling scheme (left) and illustration of parallel plate capacitor model (right).

where t_0 – maximum cohesive traction, δ_0 - critical separation at initiation of damage, t_n and δ_n – normal traction and normal separation, respectively; t_r, t_s and δ_r, δ_s – two (in r and s directions) tangential tractions and separations, $\langle\delta_n\rangle = (\delta_n + |\delta_n|)/2$ – MacAulay brackets.

The physical properties of the cohesive zone are defined by the TSL $t(\delta)$.

The total energy dissipated by the cohesive element under monotonic loading conditions can be calculated by the formula

$$\Gamma_0 = t_0\delta_0 \int_0^\infty t(\delta)d\delta. \tag{10}$$

Γ_0 is equal to the critical energy-release rate for the piezoelectric/ferroelectric material.

Loading beyond maximum cohesive traction leads to initiation and evolution of the irreversible damage. Following the damage locus, the damage variable D

$$D = 1 - e^{-\langle\delta_{\max}-1\rangle}, \tag{11}$$

is increased from 0 at $\delta = 1$ to 1 for infinite separation (see Fig. 5). $\delta_{\max}$ is maximum effective separation achieved so far.

For the exponential TSL a cohesive potential function is implemented [13]:

$$\Gamma(\delta, D) = \frac{t_0\delta_0}{F(D)}\left(e - (1 + \delta F(D))e^{1-\delta F(D)}\right), \tag{12}$$

where $F(D) = \frac{W\left((1-D)(\ln(1-D)-1)/e\right)}{\ln(1-D)-1}$ and W(z) is the Lambert function.

The function $F(D)$ describes a nonlinear unloading behavior in contrast to linear unloading towards the origin usually assumed in the literature.

Normal (n) and tangential (r and s) traction coordinates are deduced as partial derivatives of Γ with respect to the corresponding separation vector components [17]:

$$t_n = \frac{\partial\Gamma(\delta, D)}{\partial\delta_n} = \frac{t_0}{\delta_0}\langle\delta_n\rangle F(D)e^{1-\delta F(D)}, \qquad t_{r(s)} = \frac{\partial\Gamma(\delta, D)}{\partial\delta_{r(s)}} = \frac{t_0}{\delta_0}\delta_{r(s)}F(D)e^{1-\delta F(D)}. \tag{13}$$

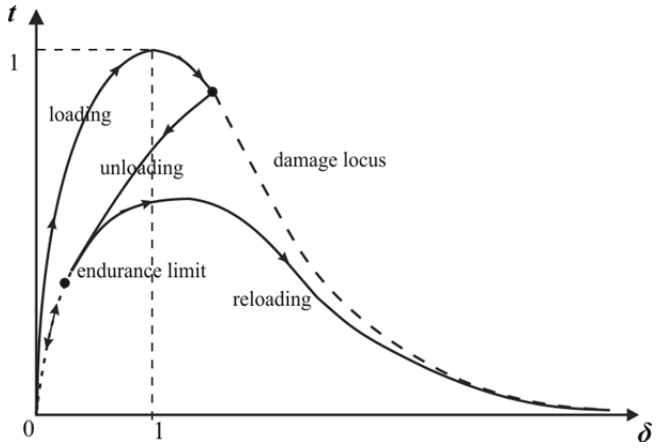

Figure 5. Features of cyclic TSL and unloading-reloading behavior.

Combining equations (10) and (13), the relation between normalized effective traction and separation can be written in the form:

$$t = \delta F(D) e^{1-\delta F(D)}. \tag{14}$$

3.3. Electromechanical coupling

It is assumed that the cohesive element possesses the properties of a medium of limited dielectric permittivity κ_c. According to [7] the opposite faces of the cohesive elements in normal direction *n* are considered as a set of parallel capacitors (Fig. 4) and the electric field inside the cohesive element can be found as

$$E_n = -[\![\varphi]\!]/\delta_n, \tag{15}$$

where $[\![\varphi]\!] = \varphi^+ - \varphi^-$ is the electric potential jump.

The idea of capacitor model is adopted to CZM [15]. Taking into account $D_n = \kappa_c E_n$ and finite thickness Δ_n of the grain boundaries [10], one arrives at the dielectric displacement field

$$D_n = -\kappa_c [\![\varphi]\!]/(\Delta_n + \delta_n) = -\omega^* \tag{16}$$

inside the cohesive elements. This equals the surface charge density ω^* at the interfaces.

The degradation of dielectric properties by damage was also accounted for by reducing the permittivity of the material during separation. Thus instead of the constant value, the effective permittivity κ_c inside the cohesive zone is assumed to degrade from undamaged value $\kappa_a = \kappa_0 \kappa_r$ to that for pure vacuum/air $\kappa_0 = 8.85 \cdot 10^{-12}$ C/V·m:

$$\kappa_c = (1-D)\kappa_a + D\kappa_0 = [(1-D)\kappa_r + D]\kappa_0. \tag{17}$$

Substituting the formula (17) in (16), the enhanced electric condition can be finally written as

$$D_n = -\big((1-D)\kappa_a + D\kappa_0\big)\frac{[\![\varphi]\!]}{\Delta_n + \delta_n}. \tag{18}$$

Using the formula (17) and taking into account that the associated crack face Coulomb tractions depend on the dielectric properties of the interior κ_c and the adjacent bulk material κ_b [16], Coulomb tractions become a function of damage *D* as

$$t_n^c = \frac{1}{2}\left(\frac{[\![\varphi]\!]}{\Delta_n + \delta_n}\right)^2 [(1-D)\kappa_r + D]\kappa_0 \left(1 - \frac{[(1-D)\kappa_r + D]\kappa_0}{\kappa_b}\right). \tag{19}$$

The relations derived above represent the complete electromechanical coupling, i.e. the influence of mechanical opening on electric charges ω^* and their feedback to mechanical response t^*.

3.4. Enhanced exponential cyclic cohesive law

The model described in subsection 3.2 is not suitable for cyclic loading with constant amplitude, because after the first cycle damage accumulation stops. Therefore, an evolution law is introduced [13] to allow cyclic damage accumulation:

$$\dot{D} = (1-D)\left(\frac{\delta}{1-\ln(1-D)}\right)^r \langle\dot{\delta}\rangle. \tag{20}$$

The endurance limit is formulated as the maximum effective traction for an infinite number of cycles

$$t_e = (1-D)^\alpha\big(1-\ln(1-D)\big). \tag{21}$$

By inverting equation (14) with respect to the effective separation δ and then substituting it into the formula (21), the expression for the endurance separation can be figured out.

As a result of introducing the endurance limit, equation (20) is extended to distinguish between active separation and endurance threshold:

$$\dot{D} = (1-D)\left(\frac{\delta}{1-\ln(1-D)}\right)^r \langle\dot{\delta}\,\mathrm{sign}(\delta - \delta_e(D))\rangle. \tag{22}$$

3.5. FEM implementation

The cohesive zone model is implemented in the commercial FE code ABAQUS© as a user element (Fig. 6). The active degrees of freedom for the cohesive element consist of one normal and two shear DOFs as well as one DOF for electric potential. The developed cohesive element can be used with arbitrary initial thickness including zero.

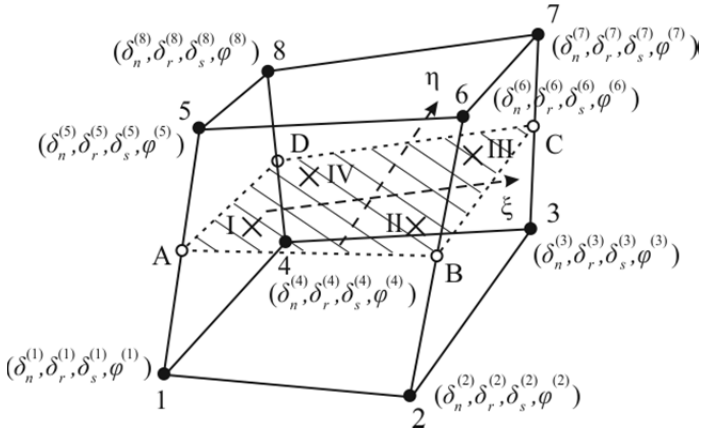

Figure 6. Three-dimensional cohesive zone element with eight nodes and four integration points.

4. NUMERICAL SIMULATION

4.1. Model validation for a test specimen

In the numerical simulations the cyclic cohesive model developed for electromechanical damage is combined with the ferroelectric bulk material which allows domain switching. The behavior of the test model is considered under uniaxial mechanical preloading followed by cyclic potential difference. The geometry of the test specimen with zero thickness CZE is presented in Fig. 7. The bulk material was modelled by the micromechanical ferroelectric law as described in Chapter 2. In the bulk material a uniform crystallographic orientation is assumed parallel to the x_3-axis. Then two states of initial polarization of all domains are prescribed either in the positive or negative x_3-direction. Ferroelectric properties of ceramics PZT-5H are used for numerical calculations. In the cohesive element the exponential cyclic TSL and generalized capacitor model are implemented. The simulations are carried out with the following parameters: G_c = 2.34 N/m, maximum cohesive traction t_0 = 80 MPa, critical separation δ_0 = $1.076 \cdot 10^{-5}$ mm. At the right hand side of the specimen, displacement and electric potential $u^0 = 0,\ \varphi^0 = 0$ are prescribed throughout the simulation. At the end of the mechanical preloading step, values of u_3^1 = 40 nm and φ^1 = 0 have to be reached at the left hand side of the specimen. In the second step an electric potential φ_c^1 alternating from 0 to 20 V is applied.

Figures 8 and 9 show the response of the specimen to the action of mechanical and cyclic electrical loading. For visualization purpose, several cycles lasting two seconds each were chosen after one second mechanical preloading. The changes in normal traction and normalized effective separation induced by mechanical and cyclic electrical loading are presented in Fig. 8.

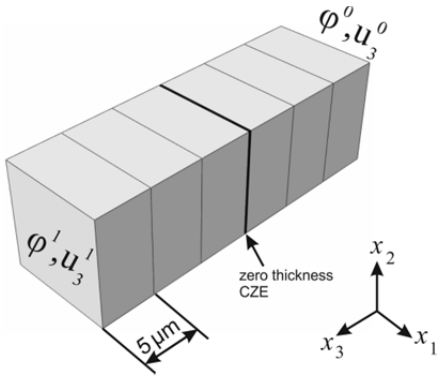

Figure 7. Test model representation.

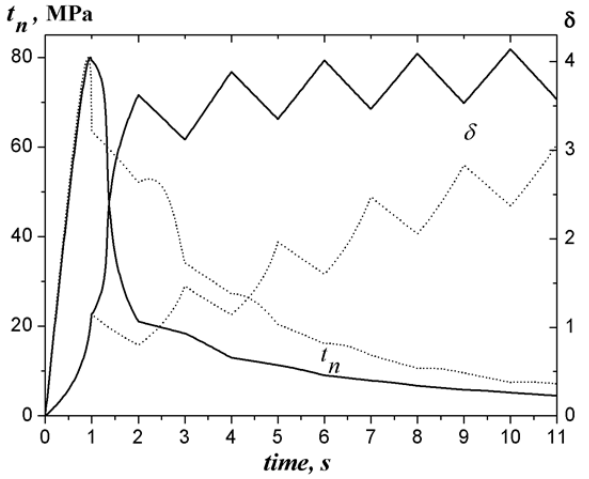

Figure 8. Changes in normal traction and normalized effective separation during mechanical and electrical loading.

Results for traction according to the TSL, introduced in Chapter 3 and graphically illustrated in Fig. 5, are presented in Fig. 9. Diagrams for the cases when polarization axis of the ferroelectric bulk material is aligned with positive and negative direction of the x_3-axis are depicted in Figs. 8 and 9 in dashed and solid lines, respectively. It can be seen from Fig. 9 that application of the electric loading along the polarization axis $+x_3$ first leads to the bulk

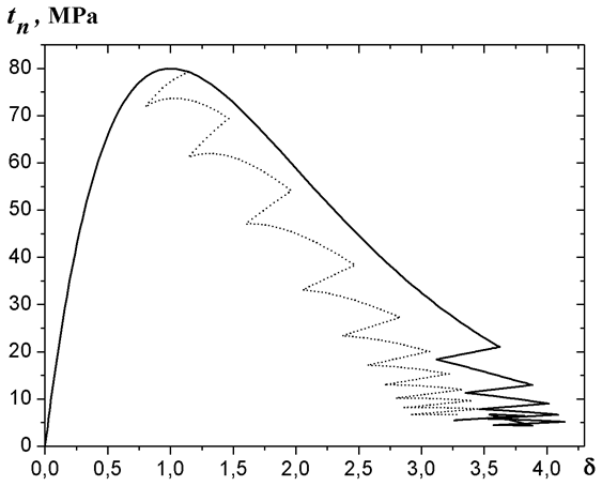

Figure 9. Response of the CZE to the mechanical preloading step followed by the electric cyclic loading.

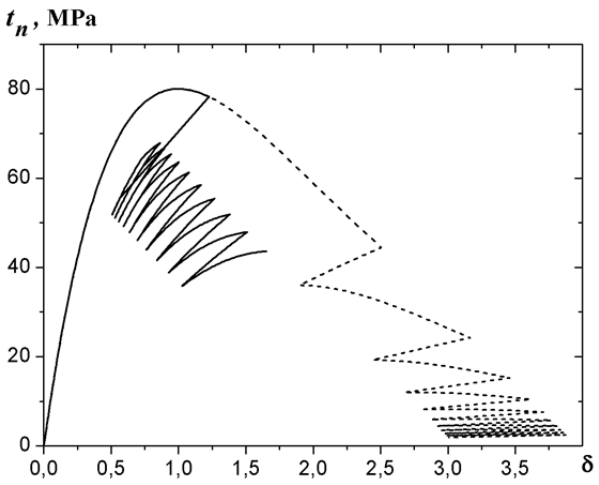

Figure 10. Response of the specimen to the electric cyclic loading taking into account domain switching.

material expansion resulting in unloading behavior in the cohesive zone. The same loading for the polarization axis $-x_3$ of the ferroelectric bulk material leads to continued loading followed by unloading-reloading with pronounced damage accumulation. It is worth to note that damage in the cohesive element after mechanical preloading step is accumulated merely due to the cyclic electric loading.

It should be recalled that the coercive field for lead zirconate titanate PZT-5H polycrystal is equal to 0.8 kV/mm. For the loading of above mentioned magnitude no switching occurs, since the maximum value of the electric potential gradient is below the coercive field.

To study the effect of domain switching jointly with the CZE behavior, the value of u_3^1 at the end of the mechanical preloading step is reduced to 33 nm while the electric potential φ_c^1 is increased to 30 V. This leads to the electric potential gradient maximum value of 1.0 kV/mm which is beyond the coercive field. In the ferroelectric bulk with the polarization axis

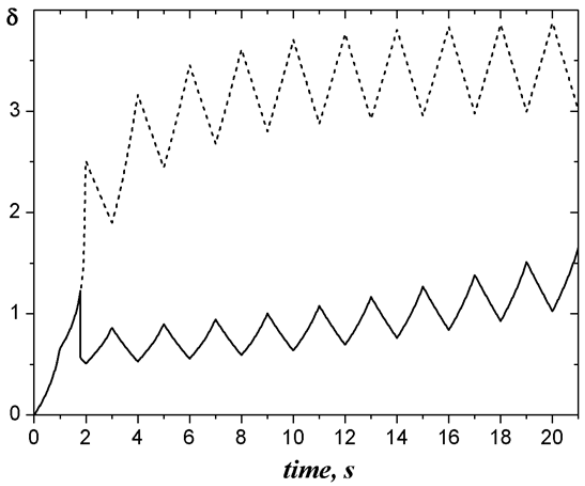

Figure 11. Difference in the normalized effective separation in cases when domain switching is considered (solid line) or neglected (dashed line).

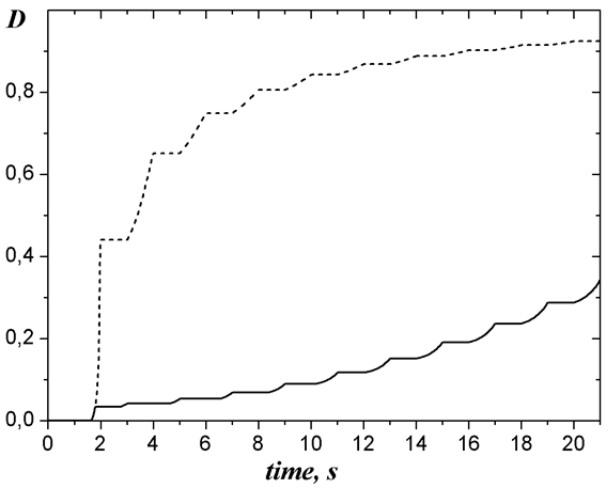

Figure 12. Difference in damage accumulation patterns when taking into account ferroelectric domain switching.

$+x_3$ no switching occurs if the applied electric potential difference is positive. In contrast, ferroelectric bulk with the polarization axis $-x_3$ experiences 180° switching under the same electrical conditions.

The comparison between the results with and without switching is presented in Figs. 10-12. Results are depicted in solid or dashed lines for the cases when the ferroelectric switching is taken into account or neglected. Once the electric potential gradient has reached the value of 0.8 kV/mm, 180° switching occurs leading to the reverse orientation of the ferroelectric bulk properties and to the prompt elongation in the direction of the x_3-axis.

This causes the sudden drop in effective separation in the cohesive zone. Starting from this moment, the behavior of the bulk material jumps from the pattern plotted in Figs. 10-12 with dashed lines to the solid ones. It could be resumed that neglect of the possible domain switching might lead to the incorrect results in the cohesive elements behavior thus influencing the validity of the numerical solution.

4.2. Crack in ferroelectric material

As an example of the cyclic cohesive model implementation the numerical simulations are performed for a crack in ferroelectric bulk material. Bulk material and cohesive elements parameters used for the simulation coincide with the parameters for the test model. The geometry of the specimen with a crack is presented in Fig. 13. The cohesive elements have zero initial thickness. Although 3-D finite elements are used, plane strain conditions in x_2 direction are imposed. Specimen is initially polarized along the positive direction of x_3 axis. It is supposed that crack is at first opened by u_3 = 0.14 μm, then the potential difference φ_c is applied: five electric cycles alternating from 0 to 40 V are followed by another five cycles alternating from 0 to 80 V.

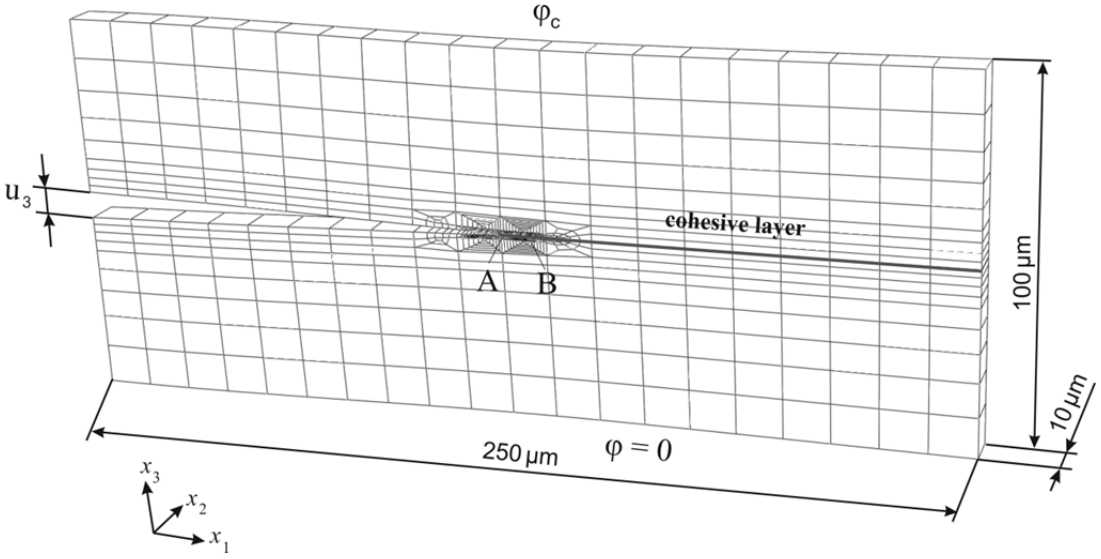

Figure 13. Crack in the ferroelectric specimen.

According to [14] below the endurance limit unloading and reloading curves match for infinite cycling and when overcoming the endurance locus, damage initiates. So electric loading has to be sufficiently strong for damage accumulation. Figure 14 illustrates the

effective traction together with damage accumulation over 10 electric cycles (2 seconds each). For the graphical representation CZE A (solid) is chosen at the crack tip, while CZE B (dashed) is at a small distance ahead of the crack tip.

It can be seen from Fig. 14 that there is damage initiation and accumulation under cyclic electrical loading with constant amplitude. According to the electromechanical cohesive zone model, unloading-reloading behaviour develops in the cohesive elements. Due to the higher stresses damage first occurs in the element A and is accumulated during cycling while in the CZE B effective traction is only slightly above the endurance limit and damage is almost zero.

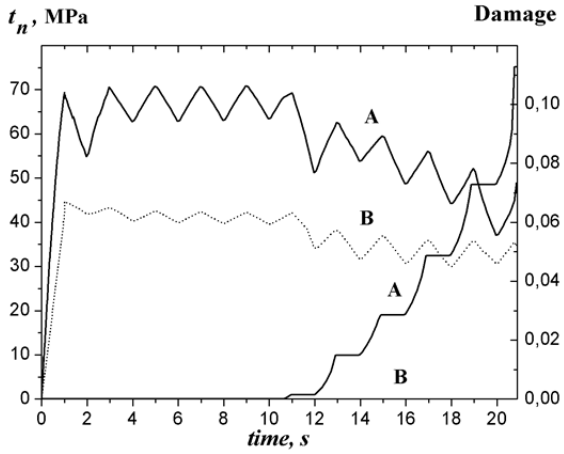

Figure 14. Changes in effective traction and damage initiation and accumulation as a result of the cyclic electric loading of different magnitudes.

5. CONCLUSIONS

In this research a coupled electromechanical cohesive model for damage simulation in ferroelectric materials is developed. The fracture of ferroelectric materials is simulated under electromechanical loading using an exponential cyclic cohesive zone model together with non-linear ferroelectric bulk material law. This approach allows for the damage accumulation during arbitrary electromechanical loading.

In the presented model the permittivity of the cohesive elements is taken into account, which degrades with increasing damage. In the cohesive elements electric potential jump is observed under mechanical opening, which in turn induces charges and Coulomb tractions on the cohesive faces.

In the numerical simulations the ferroelectric domain switching is taken into account and investigated depending on the magnitude of the applied cyclic electric field. The realistic impact of the cyclic electric field on the fracture of the ferroelectric specimen is observed: change in polarization in the domains influences the response of the specimen to the loading, including damage magnitude and accumulation speed. It is stated that neglect of a possible domain switching might lead to incorrect prediction of damage in cohesive elements.

As an example of possible model applications the numerical simulations are performed for a crack in ferroelectric bulk material. The results show realistic cyclic electric field influence on the damage initiation and accumulation near the crack tip.

The developed cohesive model forms a basis for simulations of fatigue and damage, occurring in the microstructure of smart ceramics as well as in smart devices.

ACKNOWLEDGMENTS

The research was funded by DFG under grant KU 929/20. Part of this work was performed within the Cluster of Excellence ADDE financially supported by the EU and by the Ministry of Science and Art of Saxony. One of the authors (S. Kozinov) acknowledges greatly the grant of the Ministry of Education, Science, Youth and Sport of Ukraine.

REFERENCES

[1] Kuna M., 2010. Fracture mechanics of piezoelectric materials - Where are we right now? Engineering Fracture Mechanics, 77 (2), 309-326.
[2] Schneider G.A., 2007. Influence of electric field and mechanical stresses on the fracture of ferroelectrics. Annual Rev Mater Res, 37, 491–538.
[3] Lupascu D.C., 2004. Fatigue in Ferroelectric Ceramics and Related Issues. Springer.
[4] Nuffer J., Lupascu D.C., Roedel J., 2000. Damage evolution in ferroelectric PZT induced by bipolar electric cycling. Acta Mater 48, 3783–94.
[5] Westram I., Ricoeur A., Emrich A., Rödel J., Kuna, M., 2007. Fatigue crack growth law for ferroelectrics under cyclic electrical and combined electromechanical loading. Journal of the European Ceramics Society 27, 2485-2494.
[6] Parton, V., Kudryavtsev, B., 1988. Electromagnetoelasticity. Gordon and Breach Science Publishers, New York.
[7] Hao T., Shen Z., 1994. A new electric boundary condition of electric fracture mechanics and its applications. Eng. Fract. Mech. 47, 793-802.
[8] Arias I., Serebrinsky S., Ortiz M., 2006. A Phenomenological Cohesive Model of Ferroelectric Fatigue. Acta Mater., 54, 975–84.
[9] Utzinger J., Steinmann P., Menzel A., 2008. On the simulation of cohesive fatigue effects in grain boundaries of a piezoelectric mesostructure, Int. J. Solids Struct., 45, 4687–4708.
[10] Verhoosel C.V., Gutierrez M.A., 2009. Modelling inter- and transgranular fracture in piezoelectric polycrystals. Eng. Fract. Mech., 76, 742–760.
[11] Li Q., Kuna M., 2012. Inhomogeneity and material configurational forces in three dimensional ferroelectric polycrystals. European Journal of Mechanics A/Solids 31, 77-89.
[12] Hwang S.C., McMeeking R.M., 1999. A finite element model of ferroelectric polycrystals. Int. J. Solids Struct. 36, 1541–1556.
[13] Roth S., Kuna M., 2011. Numerical Study on Interfacial Damage of Sprayed Coatings due to Thermo-mechanical Fatigue. In: XI International Conference on Computational Plasticity. Fundamentals and Applications. Ed. by Onate E. and Owen D.R. J.
[14] Roth S., Hütter G., Kuna M., 2014. Simulation of Fatigue Crack Growth with a Cyclic Cohesive Zone Model. Int. J. Fracture [accepted for publication].
[15] Kozinov S., Kuna M., Roth S., 2014. A cohesive zone model for the electromechanical damage of piezoelectric/ferroelectric materials. Smart Mater. Struct. 23 (2014) 055024.
[16] Ricoeur A., Kuna M., 2009. Electrostatic traction at dielectric interfaces and their implication for crack boundary conditions. Mech. Research Communications 36, 330-335.
[17] Bouvard J., Chaboche J., Feyel F., Gallerneau F., 2009. A cohesive zone model for fatigue and creep-fatigue crack growth in single crystal superalloys. Int Journal of Fatigue, 31(5), 868–879.